ENCIT 2018

ABCM Associação Brasileira de Engenharia e Ciências Mecânicas

17th Brazilian Congress of Thermal Sciences and Engineering
November 25th-28th, 2018, Águas de Lindóia, SP, Brazil

ENCIT-2018-0317
NUMERICAL SIMULATION OF NATURAL CONVECTION OVER A HORIZONTAL PLATE

Mario Cesar Ito
Vicente Luiz Scalon
Universidade Estadual Paulista "Júlio de Mesquita Filho",Department of Mechanical Engineering, Bauru-SP, Brazil
mario.ito@unesp.br
scalon@feb.unesp.br
Patrick H Oosthuizen
Queen's University, Kingston-ON, Canada
oosthuiz@queensu.ca

Abstract. *This study intends to solve numerically the problem of heat transfer by natural convection over a flat horizontal surface. The simulations were made by a range of Rayleigh values varying from* $10^4 \leq R_a \leq 10^9$*. The software used to run the simulations was the OpenFOAM®, which is a open source CFD modelling software. Then the results for average Nusselt number are compared with experimental correlations. A brief discussion about the behavior of the boundary layer is also presented.*

Keywords: *natural convection, heat transfer,simulation, OpenFOAM®.*

Nomenclature

Abbreviations

avg	Average
sim	Simulated

Greek symbols

α	Thermal diffusivity $[m^2/s]$
β	Gas expansion coefficient $[1/K]$
δ	Boundary layer tickness
ν	kinematic viscosity $[m^2/s]$
ρ	Specifc mass $[kg/m^3]$
τ	Dimensionless time
θ	Dimensionless temperature

Symbols

g	Gravity aceleration $[m/s^2]$
Gr	Grashof number
H	Height of the domain
h	Heat transfer coefficient $[W/m^2K]$
k	Thermal conductivity $[W/mK]$
L	Plate lenght $[m]$
n	Normal direction
Nu	Nusselt number
p	Pressure $[Pa]$
Pr	Prandtl number
Ra	Rayleigh number
T	Temperature $[K]$
v	Velocity $[m/s]$
W	Lenght of the domain
x	x direction $[m]$
y	y direction $[m]$
z	z direction $[m]$

Superscript

$*$	Dimensionless

Subscriptions

∞	Environment
i	General direction
p	Plate
s	Surface
T	Thermal
x	x direction
y	y direction
z	z direction

1. INTRODUCTION

The heat transfer by natural convection is a phenomenon that occurs in many equipments, devices, and systems of engineers interest, for example electronic components in electronic circuits, photovoltaic panels, solar thermal collectors, roofs, thermal load from ambients and etc.

The natural convection over a flat horizontal plate is a problem that has been studied for many decades and a large number of empirical correlation are available in literature (Dascalaki *et al.*, 1994). Table 1 present some of them.

The majority of this expression were deduced from correlations with experimental procedure made with an isothermal horizontal plate. In this kind of experiment the working fluid removes heat from the plate (Fishenden and Saunders, 1950; Al-Arabi and El-Riedy, 1976; Kitamura *et al.*, 2015).

Another type of experimental procedure was the mass transfer experiments (Lloyd and Moran, 1974; Goldstein *et al.*, 1973).

Table 1. Experimental correlations of average Nusselt number for horizontal flat plates.

N^o	Ra range	Equation	Equation Author
I	$Ra < 10^9$	$Nu_{avg} = 0.54Ra^{1/4}$	(Fishenden and Saunders, 1950)
II	$Ra \geq 10^9$	$Nu_{avg} = 0.14Ra^{1/3}$	
III	$10^5 \leq Ra < 10^7$	$Nu_{avg} = 0.54Ra^{1/4}$	(Lloyd and Moran, 1974; Goldstein *et al.*, 1973)
IV	$10^7 \leq Ra < 10^{10}$	$Nu_{avg} = 0.15Ra^{1/3}$	
V	$2\,10^5 < Ra \leq 4\,10^7$	$Nu_{avg} = 0.70Ra^{1/4}$	(Al-Arabi and El-Riedy, 1976)
VI	$Ra > 4\,10^7$	$Nu_{avg} = 0.155Ra^{1/3}$	
VII	$10^4 \leq Ra \leq 2\,10^6$	$Nu_{avg} = 1.65Ra^{0.175}$	(Kitamura *et al.*, 2015)
VIII	$2\,10^6 < Ra \leq 7\,10^7$	$Nu_{avg} = 0.48Ra^{0.26}$	
IX	$7\,10^7 \leq Ra < 3.5\,10^8$	$Nu_{avg} = 0.135Ra^{0.33}$	

Some expressions presented in Tab. 1 are identical with exception of the range of Rayleigh number which the correlation are applicable.

A special attention for the expressions given by Kitamura *et al.* (2015) because they did experiments for various aspect ratios of length x width, the correlations presented by this author are those that fit for all the aspect ratios evalueted by them.

As seen in Tab 1 the correlations for Nusselt number reach some transition value. This transition is assumed to occur in Ra $\approx 10^7$ (Clear *et al.*, 2003). Assumed to be a laminar to turbulent flow transition.

Studies of numerical model of heat transfer in horizontal plates confined in an enclosure domain were developed by Pretot *et al.* (2000); Venturi *et al.* (2005); Altaç and Konrat (2009). In their works they achieve good correlations when compared with experimental results.

This studied intend to simulate the natural convection phenomena over a flat horizontal plate with the open source CFD software OpenFOAM®. The configured domain has open boundaries allowing the fluid flux enter and exit the boundaries.

2. MATHEMATICAL FORMULATION

Considering the Navier-Stokes equation applied to natural conection regarding to the Boussinesq hipoteses, the balance of mass, momentum and energy are given by:

$$\frac{\partial v_x}{\partial x} + \frac{\partial v_y}{\partial y} + \frac{\partial v_z}{\partial z} = 0$$

$$\frac{\partial v_i}{\partial t} + v_x\frac{\partial v_i}{\partial x} + v_y\frac{\partial v_i}{\partial y} + v_z\frac{\partial v_i}{\partial z} = \nu\left(\frac{\partial^2 v_i}{\partial x^2} + \frac{\partial^2 v_i}{\partial y^2} + \frac{\partial^2 v_i}{\partial z^2}\right) - \frac{1}{\rho}\frac{\partial p}{\partial x_i} + \beta\,(T - T_\infty)g_i$$

$$\frac{\partial T}{\partial t} + v_x\frac{\partial T}{\partial x} + v_y\frac{\partial T}{\partial y} + v_z\frac{\partial T}{\partial z} = \alpha\left(\frac{\partial^2 T}{\partial x^2} + \frac{\partial^2 T}{\partial y^2} + \frac{\partial^2 T}{\partial z^2}\right)$$

where the i terms change with the direction on momentum equation.

Introducing dimensioneless variable as:

$$u^* = \frac{v_x\,L}{\nu}, v^* = \frac{v_y\,L}{\nu}, w^* = \frac{v_z\,L}{\nu}, x^* = \frac{x}{L}, y^* = \frac{y}{L}, z^* = \frac{z}{L}, p^* = \frac{p\,L^2}{\rho\,\nu^2}$$

$$Gr_i = \frac{g_i\,\beta\,(Ts - T_\infty)\,L^3}{\nu^2}, \tau = \frac{\nu\,t}{L^2}, \theta = \frac{T - T_\infty}{Ts - T_\infty}, P_r = \frac{\nu}{\alpha}, Nu = \frac{h\,L}{k}$$

the dimensionless equations are changed to:

$$\frac{\partial u^*}{\partial x^*} + \frac{\partial v^*}{\partial y^*} + \frac{\partial w^*}{\partial z^*} = 0$$

$$\frac{\partial {v_i}^*}{\partial \tau} + u^* \frac{\partial {v_i}^*}{\partial x^*} + v^* \frac{\partial {v_i}^*}{\partial y^*} + w^* \frac{\partial {v_i}^*}{\partial z^*} = \left(\frac{\partial^2 {v_i}^*}{\partial {x^*}^2} + \frac{\partial^2 {v_i}^*}{\partial {y^*}^2} + \frac{\partial^2 {v_i}^*}{\partial {z^*}^2} \right) - \frac{\partial p^*}{\partial {x_i}^*} + Gr_i\, \theta$$

$$\frac{\partial \theta}{\partial \tau} + u^* \frac{\partial \theta}{\partial x^*} + v^* \frac{\partial \theta}{\partial y^*} + w^* \frac{\partial \theta}{\partial z^*} = \frac{1}{P_r} \left(\frac{\partial^2 \theta}{\partial {x^*}^2} + \frac{\partial^2 \theta}{\partial {y^*}^2} + \frac{\partial^2 \theta}{\partial {z^*}^2} \right)$$

For the boundary conditions, they need to be adjust by converting to dimensionless conditions. A important condition used in these case to evaluate the heat transfer coefficient is:

$$h\,(Ts - T_\infty) = -k\,\frac{\partial T}{\partial n}$$

which could be expressed on a dimensionless form as:

$$Nu = -\frac{\partial \theta}{\partial n^*}$$

where n^* represents que normal coordinate of the boundary being analysed.

3. NUMERICAL MODEL

Two model are defined to run these simulations the first one was for the laminar cases and for this model, simulations for Ra from 10^4 to 10^6 were runned. The second model was for the turbulence cases where Ra was simulated for 10^7 until 10^9 . Both model are 2-dimensional cases, steady-state and the temperature of the plate is consider as isothermal.

Simulations were runned as dimensionless cases, as presented in mathematical model. To achieve the right Rayleigh number the value of gravity was set to the value of the Grashof number for each case .

The following sub sections present the boundary conditions and simulation settings in OpenFOAM®, for both laminar and turbulent cases then a grid setup is explained.

3.1 Laminar case

For the laminar case which was simulated for $10^4 \leq\ Ra\ \leq 10^6$ the model are compound by the following boundary surfaces and boundary conditions presented in Tab 2

Table 2. Boundary conditions for laminar case.

	openSurface	plate	base	symmetryPlane
θ (Temperature)	inletOutlet	$\theta = 1$	$\partial\,\theta/\partial\,n = 0$	symmetry
u^*, v^* (Velocity)	pressure based velocity	noSlip	slip	symmetry
p^* (Pressure)	meanValue	fixed Flux	fixed Flux	symmetry

The inletOutlet boundary condition sets the patch value to a specified value for reverse flow and to outflow it treats the boundary as zero gradient.

The pressure based velocity or pressureInletOutletVelocity as named in OpenFOAM®, is a boundary condition applied to a boundary where the pressure is specified. A zero gradient condition is applied to outflow. To inflow, the velocity is obtained from the patch-normal component of the cell.

The fixed mean condition extrapolates the value of field to patch using near cell values, and adjusts the distribution to match the specified mean value.

The openFoam setting to run this laminar simulations were the first order upwind discretization scheme, under relaxation factor of 0.3 for pressure 0.7 for momentum and 1.0 for energy.

To check if the model is converged verifications were made in the domain to see if the cells near the plate achieve the steady state condition. To assume certain pattern these simulations were runned for 15000 iterations.

The solver for these cases was the buoyantBoussinesqSimpleFoam, which is an steady state, incompressible with Buossinesq's approximation and uses the SIMPLE algorithm to couple the pressure and velocity.

3.2 Turbulent case

The turbulence cases were those that the Ra range are 10^7 until 10^9. The same boundary conditions were implemented to dimensionless temperature, velocity and pressure.

For the turbulence model the $k - \epsilon$ model was selected. This model is one of the most used in CFD modeling. The model added more two transport equation to be solved while solving the problem. One of this equation is for k which is the turbulent kinetic energy and another is for ϵ which is the turbulent energy dissipation.

The simulations settings like, solver, under relaxation factor and discretization schemes used to run this turbulent cases were the same as those used to run the laminar case.

The number of iterations was increased to 40000 iterations which was an over estimated number of iterations, but with this number we ensure that the steady state was achieved. The same verifications on the fields were made after the simulation was finished to guarantee that the solution had been converged.

3.3 Grid

The dimensions of the domain are H=L$= 5m$ and $x_p = 0.5m$. The domain has the following patches presented in Tab 3.

Table 3. Description of the boundaries.

Boundary	Description
openSurface	Right and top boundaries. These boundaries are a open patch were the flow can in and out. Simulating an open atmosphere condition;
plate	Boundary where the air is in contact with the half of the plate;
base	Floor adjacent to the plate;
symmetryPlane	Boudary related to the simmetry plane in the middle of the plate.

The Fig 1 shows the dimensions markers and the boundaries names.

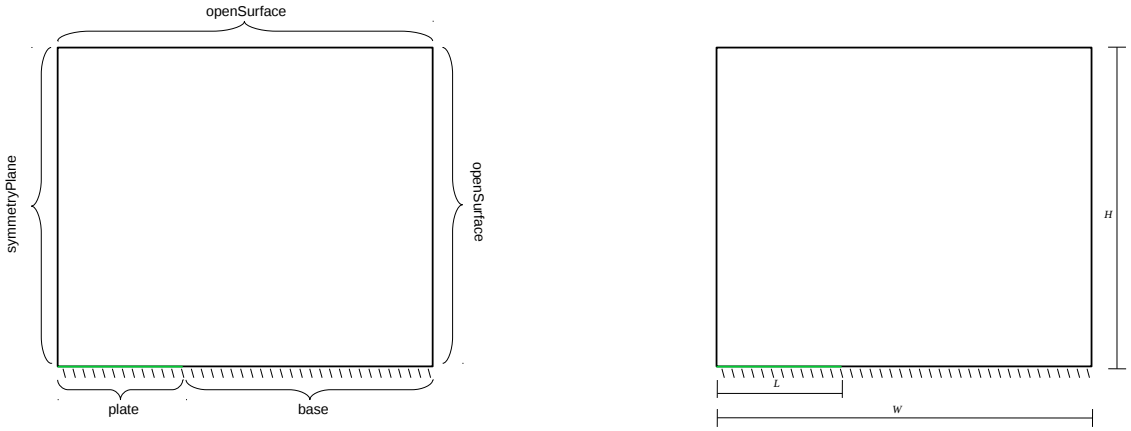

Figure 1. Boundary and dimensions for the simulated domain

A regular hexahedral mesh was used to run theses cases. The mesh was constructed with the application blockMeshDict which is a native mesh constructor of OpenFOAM®.

The mesh was build with two blocks, the first block has the dimensions $L\ X\ H$ and the second block has $(W-L)\ X\ H$. To configure the ideal grid that return not only qualitative results but also quantitative results, three meshes were studied at beginning of the simulations. The first one with 20000 volumes, the second with 80000 and the third with 500000 volumes.

The two blocks that configure the domain always have the same number of volumes, for example the grid with 80000 elements is composed by two blocks of 200x200 elements. This condense the number of elements in the region where the phenomenon occurs and let the grid more coarse in the regions far from the plate.

To emphasize even more this condense effect and to guarantee that the boundary layer is being discretized with a sufficient number of volumes, some local refinement was made in the y direction and in x direction. The y refinement was made from the plate region to the top. The x refinement was made in two directions. The first one from leading edge of the plate to center of the plate. The second one from leading edge to the right boundary which is a openSurface patch.

The simulations for the three cases were runned for the same conditions, and to visualize the grid convergence the local Nusselt number was plotted for the three cases and showed in the Fig 2.

Assuming that the most refined mesh leads to a precise results, the comparisons were made taking this most refined

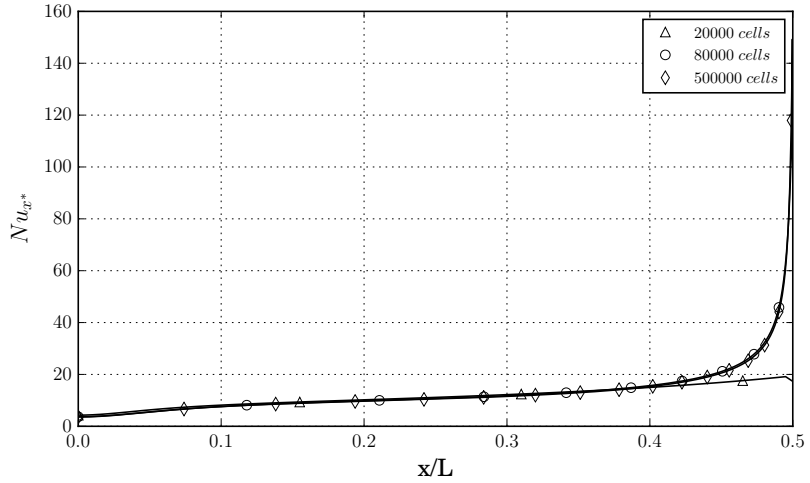

Figure 2. Grid test for 20000,80000 and 500000 cells. Result for Nu_{avg}.

mesh as reference. As seen in the Fig 2 for the coarse mesh from $x/L = 0.4$ the result start to diverge when compared with the reference refined mesh. Table 4 shows the error for the average Nusselt for the three cases.

Table 4. Average Nusselt for each tested grid and relative error when compared with most refined mesh.

N^o of cells	Nu_{avg}	Error[%]
20000	11.43	42.6
80000	20.15	1.20
500000	19.91	0.00

Making this procedure the mesh with 80000 elements will be used in all subsequently simulations because its offer advantage relation of qualitative and quantitative results by the simulations time.

4. RESULTS

Figure 3 shows how the θ and u^* field looks like after the simulation was complete. All the simulations had the same behavior, with the plume formed in the center of the plate and as the Ra was increases the thermal boundary layer became thinner.

For the u^* field it is possible to notice that the velocity profile also appears in the plate and it increase his thickness to a maximum value then start to decrease as goes nearest the center of the plate.

The results section will be divided into two sub section the first one to laminar cases and the second for the turbulence cases.

4.1 Laminar results

The profiles of θ and u^* are plotted in Figs 4 and 5.

The top x/L scale refers to the position in the plate which the profiles were taken that were at $x/L = 0.45, 0.3, 0.15$, where 0.45 is closest to leading edge and 0.15 closest to center.

The bottom scale refers to θ or u^* and they have ticks labels like $1/0$ or $0/-180$ this labels are due to each graphic has three bottom scales. Then the number to right side of the slash refers to the curves in the right side of the tick, and for the number in left side of the slash refers to the curves in left side of the tick.

The filled marker points in the θ profiles indicate where the θ achieves the value of 0.01 which delimits the thermal boundary layer. This values are reported in Tab 5.

Notice that for $Ra = 10^4$ the θ value does not go to 0.01 in any of the three positions. This also happens with results of θ for $Ra = 10^5$ and 10^6 in $x/L = 0.15$ position. The reason why this happens is because the thermal plume perturbates the temperature field nearest the plate, and as lower is the Ra values, larger the thermal plume is and sooner in x/L direction the plume starts to goes up. This fact comproves the increasing in the advective effects as Ra increases, therefore a larger Nusselt number is expected.

With effect of the perturbations in the θ field the u^* field will also suffer some consequences. For example by the effect of elevation of the plume, the free stream velocity above the plate does not converge to the same velocity, because nearest

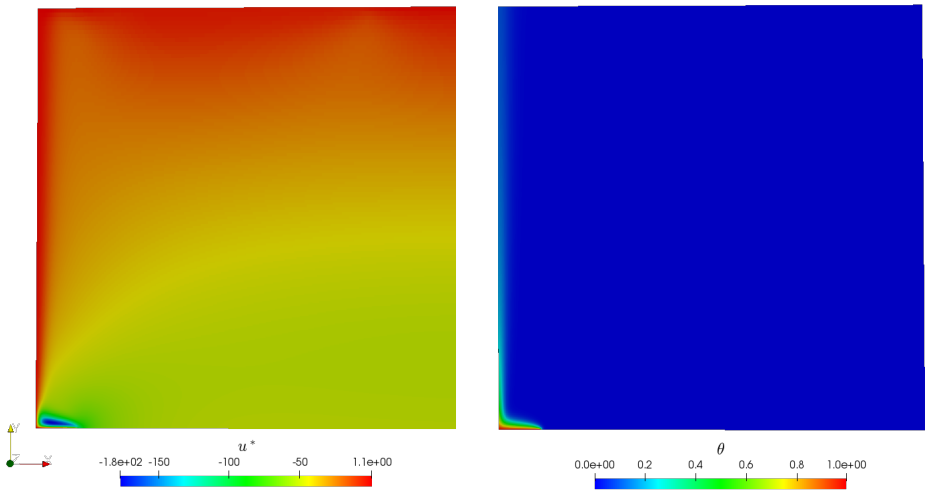

Figure 3. θ and u^* field for $Ra = 10^6$

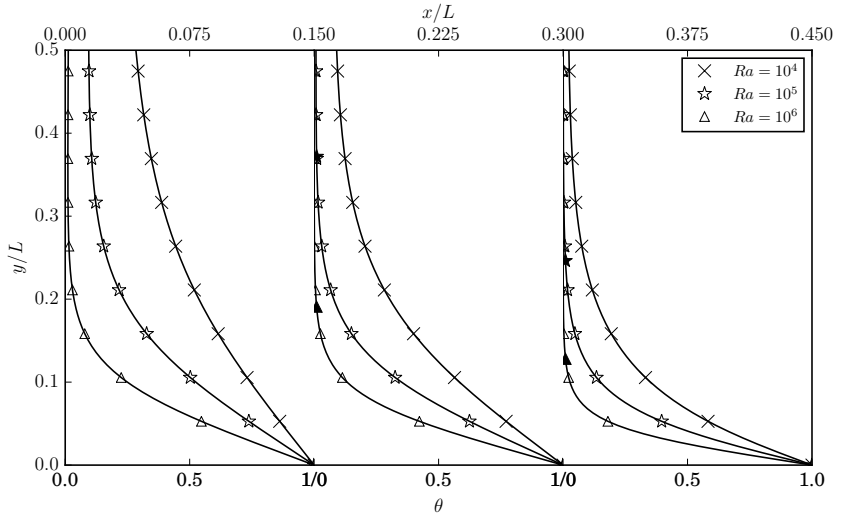

Figure 4. Development of thermal boundary layer for Ra = 10^4,10^5 and 10^6. Profiles taked at $x/L = 0.15$, 0.30 and 0.45.

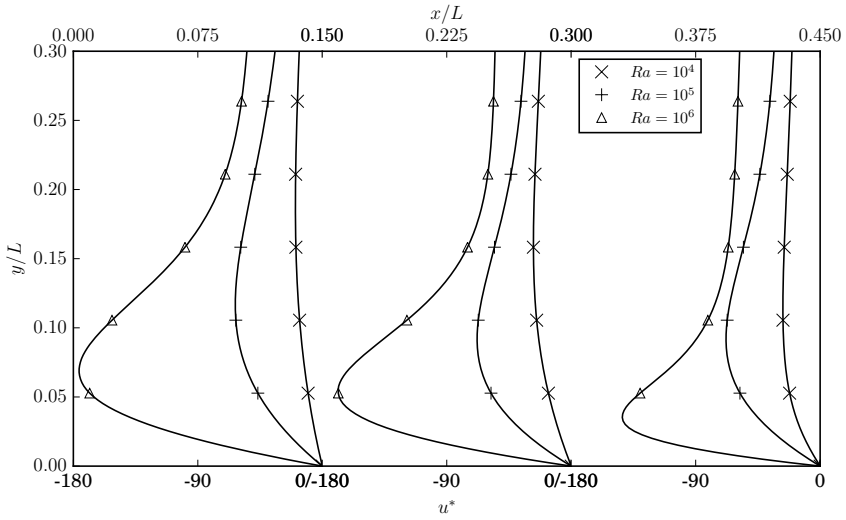

Figure 5. Development of velocity profile for Ra = 10^4,10^5 and 10^6. Profiles taked at $x/L = 0.15$, 0.30 and 0.45.

Table 5. Thermal boundary layer tickness (δ_T) for Ra in a x/L position

Ra	Position (x/L)	Boundary layer tickness (δ_T)
10^5	0.30	0.372
	0.45	0.246
10^6	0.30	0.191
	0.45	0.128

to the center of the plate the flux changes its direction creating a drag force and slowing down and this is represented by the lowers velocity and non uniformity of the free stream flux. This physical effect makes difficult to establish a limit for the hydrodynamic boundary layer since for positions nearest the center the values of the velocity will converge to different values and for the region near the leading edge the convergence will be to another values.

Tables 6, 7, 8, present the average Nusselt number for the simulations and compare the result with some related empirical expression and present the relative error.

Table 6. Results for $Ra = 10^4$.

Author	Nu_{avg}	Nu_{sim}	Relative Error [%]
(Fishenden and Saunders, 1950)	5.40	8.38	55.10
(Alamdari and Hammond, 1983)	5.72	8.38	46.41
(Kitamura *et al.*, 2015)	8.27	8.38	1.28

Table 7. Results for $Ra = 10^5$.

Author	Nu_{avg}	Nu_{sim}	Relative Error [%]
(Fishenden and Saunders, 1950)	9.60	12.90	34.34
(Alamdari and Hammond, 1983)	10.25	12.90	25.85
(Lloyd and Moran, 1974; Goldstein *et al.*, 1973)	9.60	12.90	34.34
(Kitamura *et al.*, 2015)	12.37	12.90	4.26

Table 8. Results for $Ra = 10^6$.

Author	Nu_{avg}	Nu_{sim}	Relative Error [%]
(Fishenden and Saunders, 1950)	17.08	20.15	17.98
(Lloyd and Moran, 1974; Goldstein *et al.*, 1973)	17.08	20.15	17.98
(Al-Arabi and El-Riedy, 1976)	22.13	20.15	8.99
(Alamdari and Hammond, 1983)	18.63	20.15	8.13
(Kitamura *et al.*, 2015)	18.51	20.15	8.82

Regarding the quantitative results presented in the average Nusselt numbers they achieved values that agrees with some authors specially Kitamura *et al.* (2015), where the maximum error between the simulated and experimental data was 8.82%.

4.2 Turbulent results

The same style of the graphs for θ and u^* profiles are presented for the turbulence cases. Figures 11 and 7 shows these plots.

The same effect of the thermal plume is noticed in these cases but here as the convective effects are higher the position $x/L = 0.15$ of the plate achieves the 0.01 value for the θ value in $Ra = 10^8$ and 10^9.

Even the convective effects being higher, this does not change the fact that the thermal plume rises at the center of the plate and this changes in the flow also did the same effects in the turbulent cases, but is less accentuated when compared to laminar cases due to a thinner plume, as the Ra increases. In other words, the thermal plume starts even more at the center, and giving more space to thermal boundary layer to develop itself in $-x/L$ direction. The thickness of the thermal boundary layer for the turbulence cases are presented in Tab 9.

The expected physics of the boundary layer also repeat for this cases. The thermal boundary layer decreases as the Ra increases and the thickness of the thermal boundary layer grows as the flow goes to the center for the same Ra.

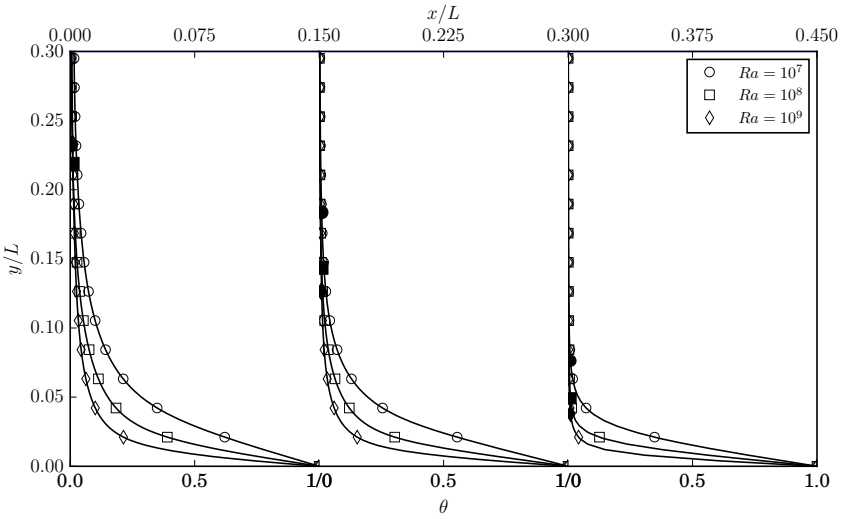

Figure 6. Development of thermal boundary layer for Ra = 10^7,10^8 and 10^9. Profiles taked at $x/L = 0.15$, 0.30 and 0.45.

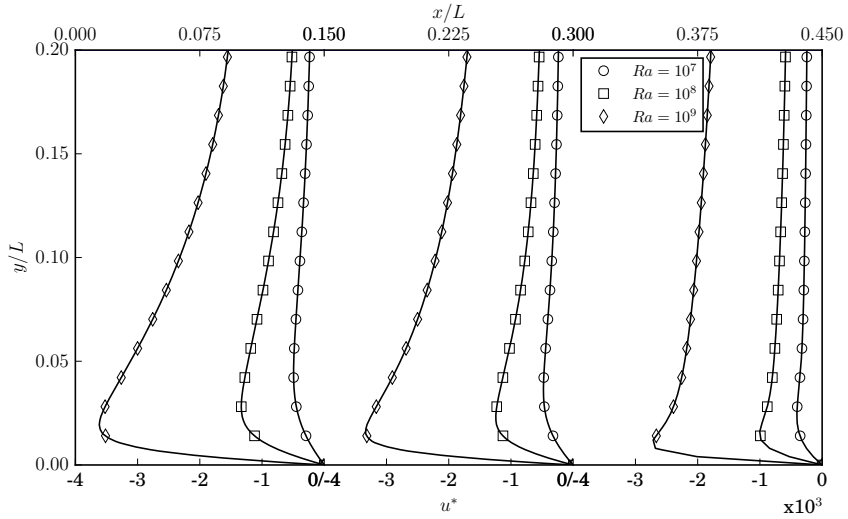

Figure 7. Development of velocity profile for Ra = 10^7,10^8 and 10^9. Profiles taked at $x/L = 0.15$, 0.30 and 0.45.

Table 9. Thermal boundary layer tickness (δ_T) for Ra in a x/L position for turbulent cases

Ra	Position (x/L)	Boundary layer tickness (δ_T)
10^7	0.30	0.184
	0.45	0.0763
10^8	0.15	0.219
	0.30	0.143
	0.45	0.0492
10^9	0.15	0.233
	0.30	0.126
	0.45	0.0381

Tables 10, 11 and 12 shows the average Nusselt number for the turbulence cases and a comparison with the empirical expressions to each Rayleigh number is presented.

The Kitamura *et al.* (2015) experimental results again gave the smallest errors, being the greatest for $Ra = 10^8$ which is 4.69%.

The errors of these turbulent cases does not ultrapass 38.47% which is a small error when compared with the 55.10% achieved in the laminar cases with Fishenden and Saunders (1950) expression for $Ra = 10^4$. But the expressions for $Ra = 10^9$ deserve an special attention due the fact that is difficult to make a controlled experiments with one Rayleigh

number so high, and the same is valid to Rayleigh number of low magnitude like 10^4. For high Ra numbers is difficult because it demands a large plate, an enough temperature difference and to make the flow stable. For the low Ra values the mainly interference comes due the fact that any perturbation in the air causes some instabilities to the measurements.

Table 10. Results for $Ra = 10^7$.

Author	Nu_{avg}	Nu_{sim}	Relative Error [%]
(Fishenden and Saunders, 1950)	30.16	33.87	4.46
(Lloyd and Moran, 1974; Goldstein *et al.*, 1973)	32.32	33.87	2.51
(Al-Arabi and El-Riedy, 1976)	39.36	33.87	19.96
(Alamdari and Hammond, 1983)	35.00	33.87	9.97
(Kitamura *et al.*, 2015)	31.71	33.87	0.65

Table 11. Results for $Ra = 10^8$.

Author	Nu_{avg}	Nu_{sim}	Relative Error [%]
(Fishenden and Saunders, 1950)	64.98	56.17	13.57
(Lloyd and Moran, 1974; Goldstein *et al.*, 1973)	69.62	56.17	19.33
(Al-Arabi and El-Riedy, 1976)	71.94	56.17	19.33
(Alamdari and Hammond, 1983)	69.18	56.17	18.81
(Kitamura *et al.*, 2015)	58.93	56.17	4.69

Table 12. Results for $Ra = 10^9$.

Author	Nu_{avg}	Nu_{sim}	Relative Error [%]
(Fishenden and Saunders, 1950)	140.00	95.37	31.88
(Lloyd and Moran, 1974; Goldstein *et al.*, 1973)	150.00	95.37	36.42
(Al-Arabi and El-Riedy, 1976)	155.00	95.37	38.47
(Alamdari and Hammond, 1983)	143.18	95.37	33.39

Figure 9 summarizes all the results of the simulations and the empirical expressions in a typical graph for the average Nusselt by the Rayleigh number. It is possible to notice that even the experimental correlations have some difference between themselves as CORCIONE (2007) mentioned in his work. But the results for the simulated values, in their majority , fit close to some experimental value. The exception is the results for $Ra = 10^9$, which diverge the most for all the experimental results.

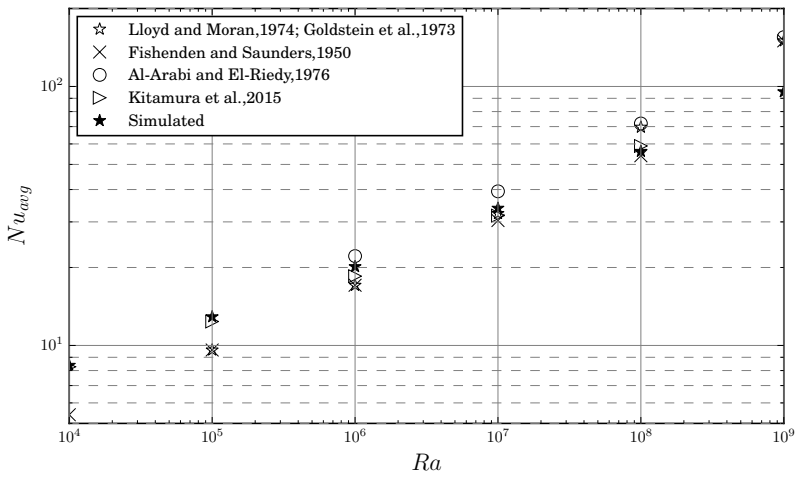

Figure 8. Rayleigh x average Nusselt graph for expressions presented in Tab 1 and simulated values

Figure 9 present the curves for the local Nusselt along the plate direction. As expected from the physic of the phenomena, the heat transfer is more intense in the leading edge of the plate and becomes smaller while it goes to center of the plate.

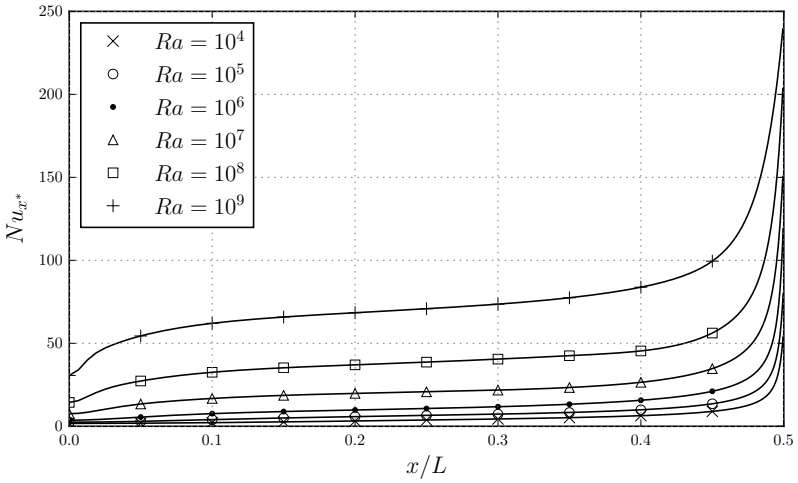

Figure 9. Local Nusselt number

5. CONCLUSION

Natural convection over a horizontal flat plate was simulated for Ra from 10^4 to 10^9 and OpenFOAM® proved to be a competent software to deal with natural convection problems. The open boundary conditions to simulate this problem works well, leading to reasonable results.

The average Nusselt number obtained for simulations from 10^4 until 10^8 are in good agreement with the experimental values found in literature. Exception was the result obtained for $Ra = 10^9$ that achieves high error values for all experimental expressions.

The physical effects are in agreement with those that were expected, the thermal plume in the center of the plate and the advective effects getting stronger as the Rayleigh number increases.

The thermal boundary layer behaves like the expected as well, increasing the thickness as the flux travels from leading edge to the center and decreasing as the Rayleigh number increases. The physical effect of the thermal plume that is not take in count by the traditional studies of boundary layer in semi-infinite flat plates, does change the hydrodynamic behavior of the boundary layer. This effect of the plume causes a change in the flow direction that affects the stream flow nearest the plate and do not allow the stream flow velocity to be converged to a single value. This fact hinders the hydrodynamic boundary layer thickness to be established.

6. ACKNOWLEDGEMENTS

The authors would like to thank the Professor Dr. Vicente Luiz Scalon and Professor Phd. Patrick H Oosthuizen for the orientation and pacience, and also thanks the UNESP for the financial support.

7. REFERENCES

Al-Arabi, M. and El-Riedy, M.K., 1976. "Natural convection heat transfer from isothermal horizontal plates of different shapes". *International Journal of Heat and Mass Transfer*, Vol. 19, No. 12, pp. 1399–1404. ISSN 0017-9310. doi:10.1016/0017-9310(76)90069-7. URL `http://www.sciencedirect.com/science/article/pii/0017931076900697`.

Alamdari, F. and Hammond, G.P., 1983. "Improved data correlations for buoyancy-driven convection in rooms". *Building Services Engineering Research and Technology*, Vol. 4, No. 3, pp. 106–112. ISSN 0143-6244. doi: 10.1177/014362448300400304. URL `https://doi.org/10.1177/014362448300400304`.

Altaç, Z. and Konrat, S., 2009. "Natural convection heat transfer from a thin horizontal isothermal plate in air-filled rectangular enclosures". *Journal of Thermal Science and Techbology*, Vol. 29, pp. 55–65. ISSN 1300-3615.

Clear, R.D., Gartland, L. and Winkelmann, F.C., 2003. "An empirical correlation for the outside convective air-film coefficient for horizontal roofs". *Energy and Buildings*, Vol. 35, No. 8, pp. 797–811. ISSN 0378-7788. doi:10.1016/S0378-7788(02)00240-2. URL `http://www.sciencedirect.com/science/article/pii/S0378778802002402`.

CORCIONE, M., 2007. "Heat Transfer Correlations for Free Convection from Upward-Facing Horizontal Rectangular Surfaces". *WSEAS Transactions on Heat and Mass Transfer*, Vol. 2.

Dascalaki, E., Santamouris, M., Balaras, C.A. and Asimakopoulos, D.N., 1994. "Natural convection heat transfer coefficients from vertical and horizontal surfaces for building applications". *Energy and Build-*

ings, Vol. 20, No. 3, pp. 243–249. ISSN 0378-7788. doi:10.1016/0378-7788(94)90027-2. URL http://www.sciencedirect.com/science/article/pii/0378778894900272.

Fishenden, M. and Saunders, O., 1950. *An Introduction to Heat Transfer*. 10. Oxford University Press, London, 1st edition.

Goldstein, R.J., Sparrow, E.M. and Jones, D.C., 1973. "Natural convection mass transfer adjacent to horizontal plates". *International Journal of Heat and Mass Transfer*, Vol. 16, No. 5, pp. 1025–1035. ISSN 0017-9310. doi:10.1016/0017-9310(73)90041-0. URL http://www.sciencedirect.com/science/article/pii/0017931073900410.

Kitamura, K., Mitsuishi, A., Suzuki, T. and Kimura, F., 2015. "Fluid flow and heat transfer of natural convection adjacent to upward-facing, rectangular plates of arbitrary aspect ratios". *International Journal of Heat and Mass Transfer*, Vol. 89, pp. 320–332. ISSN 0017-9310. doi:10.1016/j.ijheatmasstransfer.2015.05.075. URL http://www.sciencedirect.com/science/article/pii/S0017931015005694.

Lloyd, J. and Moran, W., 1974. "Natural convection adjacent to horizontal surface of various platforms". *ASME Journal of Heat and Mass Transfer*, Vol. 96, No. 12, pp. 443–447.

Pretot, S., Zeghmati, B. and Le Palec, G., 2000. "Theoretical and experimental study of natural convection on a horizontal plate". *Applied Thermal Engineering*, Vol. 20, No. 10, pp. 873–891. ISSN 1359-4311. doi:10.1016/S1359-4311(99)00067-8. URL http://www.sciencedirect.com/science/article/pii/S1359431199000678.

Venturi, D., Pulvirenti, B. and Salvigni, S., 2005. "Direct numerical simulation of natural convection over horizontal plates". In *Atti del XXIII congresso nazionale dell'Unione Italiana di Termofluidodinamica (UIT)*. Parma, Italy, pp. 365–370.

8. RESPONSIBILITY NOTICE

The authors are the only responsible for the printed material included in this paper.